Chemical Engineering Journal 263 (2015) 231–238

Contents lists available at ScienceDirect

Chemical Engineering Journal

journal homepage: www.elsevier.com/locate/cej

Toughened polystyrene nanoparticles through high-solids miniemulsion polymerization

Ludmila I. Ronco [a], Roque J. Minari [a], Mario C.G. Passeggi Jr. [b], Gregorio R. Meira [a], Luis M. Gugliotta [a,*]

[a] INTEC (Universidad Nacional del Litoral-CONICET), Güemes 3450, 3000 Santa Fe, Argentina
[b] IFIS (Universidad Nacional del Litoral-CONICET), Güemes 3450, 3000 Santa Fe, Argentina

HIGHLIGHTS

- Synthesis of toughened nanoparticles through high solid miniemulsion polymerization.
- Toughened polystyrene with controlled microstructure and nanomorphology.
- The nanostructured toughened polystyrene exhibits improved mechanical properties.

ARTICLE INFO

Article history:
Received 2 June 2014
Received in revised form 28 October 2014
Accepted 6 November 2014
Available online 11 November 2014

Keywords:
Miniemulsion polymerization
High-solids content
Toughened polystyrene
Polybutadiene

ABSTRACT

Polystyrene nanoparticles toughened with polybutadiene were synthesized by miniemulsion polymerization of 50% solids content. The effects of recipes and reaction conditions on the polymerization kinetics, polymer microstructure, particle morphology, and mechanical properties of the produced thermoplastic materials, are discussed. The final material characteristics are strongly dependant on the chemical nature of the employed initiator, and an interpretation for the observed effects is presented. The obtained nanostructured polystyrenes exhibit mechanical properties similar to those of the commercial HIPS, but with the typical advantages of polymerizations in disperse medium such as low environmental impact, high monomer conversion, and fast heat transfer.

© 2014 Published by Elsevier B.V.

1. Introduction

Mechanical properties of fragile polymers such as impact fracture are improved by incorporation of dispersed rubber particles into the main vitreous matrix. Such particles act as stress concentrators and facilitate a more uniform dispersion of the applied mechanical energy [1,2]. High-impact polystyrene (HIPS) is commonly produced in continuous bulk (or quasi-bulk) processes, where, styrene (St) is polymerized at 90–250 °C in the presence of 5–10 wt% of a dissolved rubber such as polybutadiene (PB) or a St-butadiene block copolymer. The initial prepolymerization stage ends at styrene conversions of around 30%. It is carried out under stirring, and in the presence of a chemical initiator to promote rubber grafting. The second (finishing) stage is unstirred (to preserve the particle morphology generated at the end of the prepolymerization), and is carried out at higher temperatures to promote initiation by thermal monomer decomposition. In continuous bulk processes, the final St conversion is approximately 75%; and the unreacted St must be removed in a final devolatilization stage [3,4]. The final product typically exhibits "salami" morphologies, with a vitreous PS matrix containing dispersed rubber particles of around 1 μm in size, that in turn contain multiple PS occlusions.

Several articles have investigated the development particle morphology in PS/PB blends (with PS as the major component), and with addition of minor fractions of styrene-butadiene copolymers. Jiang et al. [5] employed simple PB-g-PS copolymers with around 1 PS branch per molecule in average. When simultaneously varying the molecular weights of the free PS and grafted PS chains, the following was observed by transmission electron microscopy (TEM) [5]: (i) the 2 phases were totally immiscible when the molecular weight of free PS was much larger than the molecular weight of the grafted PS branches; (ii) the degree of mixing improved when the molecular weight of the grafted PS chains became closer to those of the free PS; and (iii) the morphology exhibited PB microdomains dispersed in the PS matrix when the molecular weight of the free PS was lower than that of the PS grafted branches. These observations are in agreement with Inoue et al. [6] and Jiang and Xie [7] for homopolymer/diblock copolymer

* Corresponding author. Tel.: +54 342 4511546; fax: +54 342 4511079.
E-mail address: lgug@intec.unl.edu.ar (L.M. Gugliotta).

http://dx.doi.org/10.1016/j.cej.2014.11.033
1385-8947/© 2014 Published by Elsevier B.V.

blends. In addition, when comparing IZOD impact resistances, it was observed that short diblock copolymers are ineffective as interface agents in PS/PB blends, while the best performance was obtained with asymmetric diblock copolymers of sufficiently high molecular weights for generating entanglements in the main interfaces [8].

Toughened PS has also been produced by blending sub-micrometer core–shell PB/PS particles into PS homopolymer [9–11]. In these experiments, the particles were obtained by emulsion polymerizations of St in the presence of a PB seed with different initiators (an oil-soluble [9], a water-soluble [11], and redox pairs [9,10]); and then such particles were blended with commercial PS, yielding blends of 20 wt% rubber content. With redox initiators, Gao et al. [9] observed that the particles contained small PS microphases inside the rubber cores, and that the obtained materials exhibited a low toughness and low impact strength. These mechanical properties were improved when employing an oil-soluble initiator (1,2-azobisisobutyronitrile), and this improvement was attributed to the larger PS occlusions generated in the rubber core [9]. Gao et al. [10] and Cai et al. [11] synthesized core–shell particles of different PB/PS ratios; observing that the degree of grafting affected both the dispersion of the rubber particles, and the mechanical properties of the final materials.

Miniemulsion polymerization of St in the presence of a rubber is an alternative for synthesizing hybrid latexes; since it incorporates hydrophobic components into the polymer particles in a single step, without requiring their diffusion through the aqueous phase. Jeong et al. [12] polymerized St in the presence of a styrene–butadiene-styrene triblock copolymer (SBS, Kraton®), added in a 20/80 weight ratio of PB rubber to St. They observed a preferential concentration of SBS in the larger particles with respect to the smaller; due to the faster nucleation of the smaller particles, combined with an additional monomer diffusion stage from the bigger particles into the smaller. Only cellular morphologies were observed, with PB-rich phases surrounded by PS-rich phases. More recently, miniemulsion polymerization was employed to obtain PS nanoparticles with different amounts of medium-cis PB or styrene-butadiene rubber (SBR) of 20% solids content [13]. The grafting efficiency and particle morphology were affected by the chemical nature of the initiator and by the molecular characteristics of the rubber; observing that increased grafting efficiencies induced more complex particle morphologies [13].

The production of high-solids latexes is industrially important; and miniemulsion polymerizations contribute toward this goal through the relatively broad particle size distributions involved, that yield low system viscosities [14–16]. The aims of this work are: (i) to synthesize PB-toughened PS nanoparticles by miniemulsion polymerization of 50 wt%. solids content; and (ii) to investigate the effects of changes in the PB concentration and in the nature of the initiation system on the polymerization kinetics, molecular microstructure, nanoparticle morphology, and mechanical properties of the final thermoplastic.

2. Experimental

2.1. Materials

The following initiators were employed as received: potassium persulfate (KPS) from Mallinckrodt (purity 99%), and benzoyl peroxide (BPO) from Akzo Nobel (Perkadox L-W75 in 25% water). Hexadecane (HD) from Aldrich (purity $\geqslant$ 99%) was the latex costabilizer; Dowfax 2EP from Dow (purity 45%) was the surfactant; tert-dodecyl mercaptan (tDM) from Fluka (purity 95%) was the chain transfer agent (CTA); and hydroquinone from Fluka (purity > 99%) was the polymerization inhibitor. Technical grade styrene was first washed with a KOH aqueous solution to remove polymerization inhibitors, and then with demineralized water until reaching the pH of the washing water. The PB was a Buna CB 55 GPT by Lanxess (medium-*cis* rubber produced by solution anionic polymerization with an organolithium catalyst). Its average molar masses were determined by size-exclusion chromatography (SEC), yielding: $\bar{M}_n$ = 142800 g/mol; and $\bar{M}_w$ = 281,200 g/mol. These values were determined through a universal calibration obtained with PS standards, and the following Mark–Houwink parameters in tetrahydrofuran at 30 °C taken from Kurata and Tsunashima [17]: (a) for PS, $K_{PS} = 1.10 \times 10^{-2}$ mL/g and $a_{PS} = 0.725$; and (b) for PB, $K_{PB} = 2.56 \times 10^{-3}$ mL/g, and $a_{PB} = 0.74$. The tetrahydrofuran SEC carrier was from J.T. Baker (HPLC Solvent). Finally, methyl-ethyl ketone (MEK, from Anedra, 99% purity) was the selective solvent for the determination of the grafted PS mass. Demineralized water was used throughout the work.

2.2. Miniemulsification

The following was common to all miniemulsions: (a) 50 wt%. of solids; (b) 5–10% wbop (weight based on organic phase) of PB; (c) 3% wbop of active surfactant; (d) 4% wbm (weight based on monomer) of HD; and (e) 0.2% wbop of $NaHCO_3$. Prior to the miniemulsifications, the following were dissolved in the monomer phase: (i) the grated PB; and (ii) the BPO initiator, and the tDM CTA (in the reactions where these reagents were employed). To produce the miniemulsion, the organic and aqueous phases were first strongly mixed by magnetic stirring during 15 min., and the resulting pre-emulsion was sonified during 45 min. in a Sonics VC 750 (power 750 watts) at 100% of amplitude, in cycles of 20 s on and 5 s off. Sonication time was determined as that required to obtain a low average droplet diameter ($\bar{d}_d$) and a narrow droplet size distribution (both measured on the miniemulsions by dynamic light scattering: DLS). Due to the high solid content and high organic phase viscosity, longer sonication times than those typically employed for St miniemulsions were needed [18]. Sonication was carried out in a refrigerated jacketed vessel, to maintain the miniemulsion temperature below 35 °C.

2.3. Polymerizations

The polymerizations were carried out in a 0.2 L batch glass reactor equipped with a reflux condenser, a stirrer, a sampling device, and a nitrogen inlet. The reaction temperature (70 or 90 °C) was adjusted by manipulation of the reactor jacket temperature, in turn controlled by a water bath. The miniemulsion was loaded into the reactor, and the system was kept under stirring and nitrogen bubbling until the desired reaction temperature was reached. Polymerizations with KPS were started by injecting its water solution as a shot. Note that while KPS generates hydrophilic radicals in the water phase, BPO generates hydrophobic radicals in the organic phase. Thus, BPO radicals are restricted to a small phase volume that enhances bimolecular termination, lowering the efficiency of those radicals with respect to the water-soluble KPS radicals [19]. For this reason, experiments involving BPO were carried out at higher temperatures, and in most cases at higher initiator concentrations. Furthermore, total polymerization times were 2 h for reactions with KPS, and 3 h for reactions with BPO.

2.4. Measurements

Prior to the reactions, the miniemulsion stability was determined in a Turbiscan TMA2000, where the intensity profile of backscattered light along a vertical tube was measured every 5 min. along 4 h; and the miniemulsion surface tension was measured with a Krüss tensiometer K8.

From the samples withdrawn along the reactions, the following measurements were carried out: (i) monomer conversion (x) by gravimetry; (ii) average droplets diameter ($\bar{d}_d$) and particles diameter ($\bar{d}_p$) by dynamic light scattering (DLS) a detection angle 90°, in a Brookhaven BI-9000 AT photometer. Prior to the DLS measurements, the samples were diluted with a water solution saturated with Dowfax 2EP and St monomer, in order to avoid droplets destabilization and loss of monomer from droplets and particles.

At the end of polymerizations, the coagulum collected from the reactor surfaces was mixed with the coagulum obtained after filtration of the latex in a 85 μm nylon mesh. The composition of the resulting coagulum was determined by ^{1}H NMR, in a Brüker Avance 300 spectrometer at 300.14 MHz. To this effect, the sample was swollen with chloroform-D_6, and its composition was calculated as described elsewhere [13].

The content of gel in the vacuum-dried polymer samples was determined by Soxhlet extraction under THF reflux along 24 h. For some samples not all the gel was retained by the paper filter during the Soxhlet extraction, and this fraction was isolated from the THF solution containing the extracted soluble polymer by centrifugation at 6000 rpm during 2.5 h. The total gel was reported as the addition of the gel fraction retained in the filter paper and that separated by centrifugation.

The grafting efficiency (E_g) and grafting degree (DG) are respectively defined as the mass of grafted St with respect to the total mass of polymerized St, and with respect to the initial mass of PB. The mass of grafted PS was determined by solvent extraction, by dissolution of the free PS in MEK, while the PB and grafted polymer remained insoluble [20]. To this effect, 0.3 g of the final dry sample was first dispersed in 10 mL of MEK, and shaken for 12 h; and then the mixture was centrifuged at 6000 rpm during 2 h. To obtain the free PS, the clear supernatant containing the dissolved PS was isolated and dried. The process was repeated again onto the undissolved fraction, in spite of most of the free PS was removed from the sample in the first extraction [13]. The remaining insoluble was dried, and E_g and DG were calculated from:

$$E_g = \frac{\text{Weight of insoluble material} - \text{Weight of initial PB}}{\text{Weight of PS in the sample}} \times 100 \quad (1)$$

$$DG = \frac{\text{Weight of insoluble material} - \text{Weight of initial PB}}{\text{Weight of initial PB}} \times 100 \quad (2)$$

The molecular weight distribution (MWD) and averages of the free PS ($\bar{M}_{n,PS}$ and $\bar{M}_{w,PS}$) were determined by SEC. The measurements were carried out with a Waters 1515 chromatograph fitted with a differential refractometer (DR, Waters 2414); and with 2 poly(St/DVB) columns (HR 4E and HR 5E from Waters Corp., of nominal fractionation range 10^3–10^7 g/mol). The chromatograph was calibrated with a set of 9 (Shodex) narrow PS standards in the range 10^3–10^6 g/mol.

The particle morphology was determined by TEM, in a JEOL 100 CX (100 kV). To this effect, the diluted latex samples were stained in liquid phase with a 2 wt% aqueous solution of Osmium tetroxide for 2 h. OsO_4 reacts with the PB double bonds, and shows a dark rubber phase. Then, a drop of the stained and diluted latex was placed on copper grids, covered with a film of polyvinyl formal (Formvar® by Fluka), and dried at room temperature. The micrographs were taken at different magnifications, depending on particle size.

To obtain the final dry polymers, 1 wt% of antioxidant was added onto the latexes, and then they were coagulated with isopropyl alcohol. The obtained bulk polymer was washed with demineralized water to eliminate the emulsifier through several cycles of centrifugation/redispersion, until the surface tension of the supernatant reached the surface tension of the washing water. Then, the wet polymer was dried under vacuum at room temperature. For the tensile tests, dumbbell-shaped specimens were obtained by compression moulding at 180 °C for 25 min. The elongation section dimensions were: length 9.53 mm, and cross section 3.18×1 mm^2. ASTMD638 tests were carried out in an universal testing machine (INSTRON 3344), at 23 °C, 50% relative humidity, and elongation rate 0.5 mm/min. At least five specimens of each sample were tested.

The internal morphology of the materials obtained by compression moulding at a temperature of 180 °C was observed with an atomic force microscope (AFM, Nanotec Electronic System) in tapping mode onto the sample transversally cut after cooling it with liquid N_2 [21]. Rotated monolithic Budget Sensors All-In-One-Al cantilevers (Budget Sensors, Sofia, Bulgaria) made of silicon with a 30 nm thick aluminum reflex coating and a tip radius <10 nm, resonance frequencies of 80 ± 30 and 150 ± 80 kHz (67.4 and 132 kHz more precisely, respectively) and nominal spring constants of k = 2.7 and 7.4 N/m were used. All the AFM experiments were performed in air at room temperature and using a scan rate of 0.6–1 Hz (lines/s). Acquisition and image processing were performed using the WS × M free software [22].

3. Results and discussions

3.1. Kinetics

Table 1 summarizes the reaction conditions, the average droplets diameter of the initial miniemulsion, and the global polymerization results obtained from final latexes. The experiment codes contain: (a) the abbreviation "PB" with a subscript indicating the polybutadiene content in % wbop; (b) the initiator name (KPS or

Table 1
Reaction conditions and measurements from the miniemulsion and final latexes.

Experiment	Temp. (°C)	$\bar{d}_d$ (nm)	x[a] (%)	$\bar{d}_p$ (nm)	$N_p \times 10^{-16}$ (#/L)	Coagulum (%)[b]
$PB_5KPS_{0.75}$	70	214	94	109	66.0	0.2
$PB_5KPS_{0.75}C_{0.4}$	70	236	97	110	99.4	0
$PB_5KPS_{0.75}C_{0.6}$	70	252	96	111	97.4	0
$PB_{10}KPS_{0.75}$	70	215	96	107	82.3	0.8
$PB_5BPO_{0.75}$	90	244	82 (96)	220	8.8	1.1
$PB_5BPO_{1.05}$	90	247	93 (95)	228	8.1	0.3
$PB_5BPO_{2.1}$	90	247	96 (96)	241	8.4	0.8
$PB_8BPO_{2.1}$	90	231	95 (95)	226	8.2	0.7
$PB_{10}BPO_{0.75}$	90	241	86 (97)	221	8.9	4.3
$PB_{10}BPO_{2.1}$	90	231	93 (94)	214	9.7	1.6

[a] x is the monomer conversion at polymerization time 2 h. In the reactions with BPO, x at 3 h is also reported in parentheses.
[b] Weight based on total latex.

BPO) with a subscript indicating its concentration in % wbm; and (c) the abbreviation "C" for the CTA with a subscript indicating its concentration in % wbm (when this last reagent was included). Thus, $PB_5KPS_{0.75}$ is indicative of an experiment with initial concentrations of PB, KPS, and CTA of 5% wbop, 0.75% wbm, and 0% wbm, respectively.

According to the Turbiscan measurements, all the miniemulsions remained stable at room temperature along 4 h. Also, the initial miniemulsion droplets ranged between 214 and 252 nm (Table 1). Even though the increase of the PB content from 5% wbop to 10% wbop caused an increase in the organic phase viscosity, it did not affect the droplet size, possibly because droplet coagulation was the determining process, i.e., the sonication power was able to break-up the droplets to smaller sizes, but such small droplets could not be stabilized by the emulsifier [23]. In all the miniemulsions, the measured values of surface tension were greater than 40 mN/m, indicating absence of emulsifier micelles (the surface tension for the DowFax 2EP solution at the CMC was 35 mN/m).

Fig. 1 presents the time evolution of the monomer conversion and particle diameter. The final monomer conversions were in all of the polymerization 94% or higher (Table 1). Compared to the experiments with KPS (at 70 °C), those with BPO (at 90 °C) produced slower polymerization rates (Fig. 1a and c), and higher final $\bar{d}_p$ values (Table 1 and Fig. 1b, d). The lower polymerization rates observed with BPO were due to the fact that those reactions exhibit lower N_p values, and considerably reduced initiation efficiencies by radical recombination. The increase in BPO content also increased polymerization rate, but did not affect the final x obtained at 3 h of reaction. For the same initiator type and concentration, the polymerization rate and $\bar{d}_p$ remained essentially unaffected by the PB content. Also, the incorporation of tDM as CTA in $PB_5KPS_{0.75}C_{0.4}$ and $PB_5KPS_{0.75}C_{0.6}$ produced a negligible effect on the final x and $\bar{d}_p$.

With KPS, $\bar{d}_p$ decreases along the polymerization (Fig. 1b) to around 110 nm. This suggests that most of the particles were generated through a secondary nucleation mechanism promoted by the hydrophilic radicals generated in the aqueous phase. Notice that the secondary nucleation mechanism is expected to be the homogeneous one, due to the absence of micelles in the initial miniemulsions. With the oil-soluble BPO, $\bar{d}_p$ remains close to $\bar{d}_d$ (Table 1 and Fig. 1d); suggesting that droplets nucleation was the main nucleation mechanism. This is because BPO radicals are formed in the monomer droplets, and exhibit low water solubility.

The presence of coagulum was observed in most experiments (Table 1). However, coagulum composition analyzed by ^{1}H NMR, exhibited a PB concentration close to that of the original PB content in the organic phase recipes. Thus suggesting that the coagulum was formed by partial destabilization of the nucleated droplets.

3.2. Polymer microstructure

Table 2 presents the total gel contents, grafting efficiency, grafting degree, and average molecular weights of the free PS (isolated by MEK extraction). Also, Table 2 presents the number of grafting points per PB chain (GP), estimated from the mass of grafted PS (E_g) and $M_{n,PS}$, with the assumption that the average chain length of the grafted PS branches coincides with that of the free PS.

As expected, the initiator nature and the particle nucleation mechanism induce large differences in the obtained products. With BPO, the gel content is considerably higher than with KPS. The miniemulsion polymerization of St without rubber does not produce gel [18], and the employed PB exhibits a negligible insoluble fraction after its extraction with THF. Thus, the gel isolated in the polymerizations with PB is basically insoluble grafted copolymer, and the gel content is expected to increase with the amount of grafting.

For the free PS, higher molecular weights were obtained in the experiments with KPS but without CTA ($PB_5KPS_{0.75}$ and $PB_{10}KPS_{0.75}$), and lower molecular weights in the experiments with BPO, even with the lowest initiator concentration (0.75% wbm). The $\bar{M}_w$ values obtained with KPS were similar to those produced in an emulsion polymerization of St without rubber, with molecular weight control by chain transfer to the monomer, and particle sizes in the range 90–130 nm [24]. However, the relatively lower values of $\bar{M}_n$ could be due to a greater contribution of termination reactions in the larger polymer particles nucleated from miniemulsion droplets, that contain a higher radical concentration. This contribution of the lower molecular weight fraction is evidenced by the important shoulder observed in the MWD of sample $PB_5KPS_{0.75}$ (Fig. 2). In addition, the fast decomposition of BPO molecules contained in large particles (of $\bar{d}_p > 214$ nm) induced an

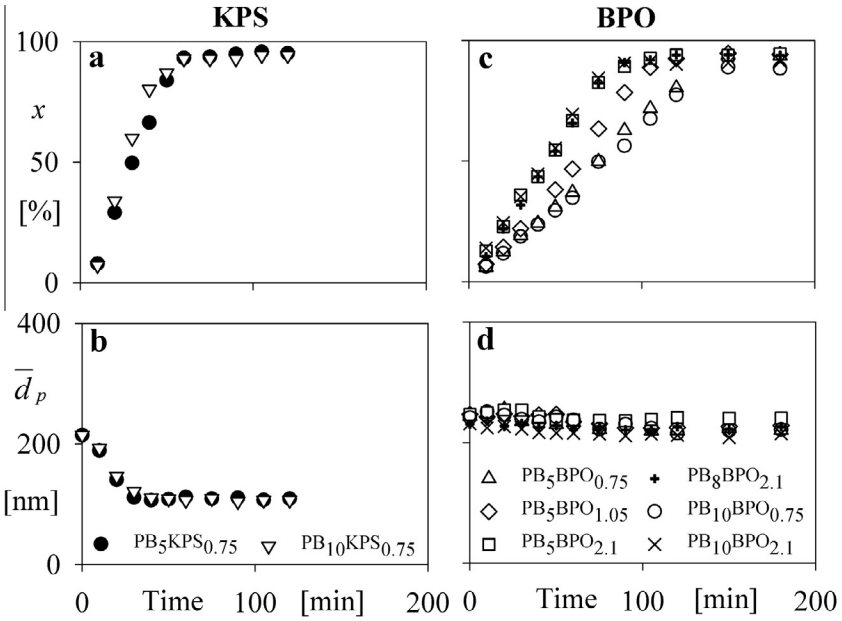

Fig. 1. Evolution of conversion (a and c), and average particle diameter (b and d) in miniemulsion polymerization of St in the presence of PB, with different initiator types (KPS or BPO) and concentrations, and varied PB contents.

Table 2
Microstructural characteristics of the final polymers.

Exp.	Total Gel (%)	E_g (%)	DG (%)	$\bar{M}_{n,PS}$ (g mol^{-1})	$\bar{M}_{w,PS}$ (g mol^{-1})	GP (#)
$PB_5KPS_{0.75}$	2.2	6.7	113	98,400	1,688,600	1.6
$PB_5KPS_{0.75}C_{0.4}$	9.3	6.8	120	30,400	242,800	5.7
$PB_5KPS_{0.75}C_{0.6}$	15.1	6.2	107	22,100	227,800	6.9
$PB_{10}KPS_{0.75}$	11.2	12.0	101	121,000	2,142,200	1.2
$PB_5BPO_{0.75}$	19.0	13.3	227	30,100	170,300	10.8
$PB_5BPO_{1.05}$	19.0	13.9	243	24,900	103,300	13.7
$PB_5BPO_{2.1}$	15.7	12.0	205	15,400	35,500	19.0
$PB_8BPO_{2.1}$	15.7	13.2	135	16,400	40,100	11.7
$PB_{10}BPO_{0.75}$	24.2	19.6	162	31,900	177,600	7.2
$PB_{10}BPO_{2.1}$	22.4	17.2	136	13,300	47,000	14.6

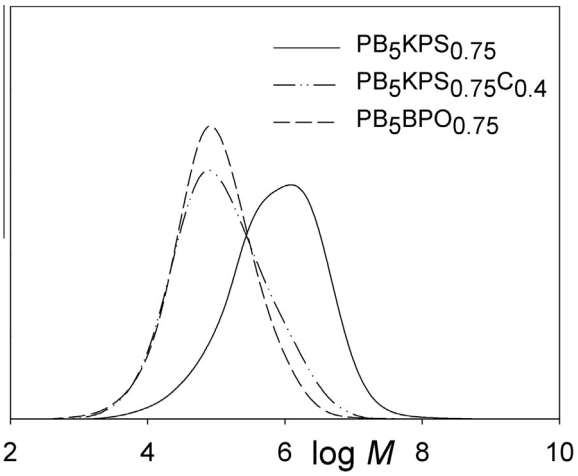

Fig. 2. MWD of the free PS obtained in the experiments $PB_5KPS_{0.75}$, $PB_5KPS_{0.75}C_{0.4}$ and $PB_5BPO_{0.75}$.

increased termination; and reduced the PS molecular weights in a polymerization system that essentially behaved as pseudo-bulk [25]. Experiments $PB_5KPS_{0.75}C_{0.4}$ and $PB_5KPS_{0.75}C_{0.6}$ with KPS and tDM were carried out to reduce the molecular weights of the free PS to values comparable to those of experiments with 0.75% wbm of BPO. The MWD of the free PS obtained when incorporating tDM in $PB_5KPS_{0.75}C_{0.4}$ exhibits low molecular weights with respect to that without tDM, and shows a single peak with a $\bar{M}_n$ value practically coincident with that of 0.75% wbm of BPO, but with a higher polydispersity (Fig. 2). Also, in $PB_5KPS_{0.75}C_{0.4}$ the MWD is much broader than that obtained under conventional batch emulsion polymerization of St with tDM [26]. This could be attributed to the low diffusion rate of the hydrophobic tDM from the droplets-nucleated particles to the secondary nucleated particles, that would generate different CTA concentrations in both kinds of particles [26]; and one can speculate that both the free PS and the grafted PS branches generated in the droplet-nucleated particles and in the presence of a higher CTA concentration, could be significantly shorter than the free PS chains generated into the secondary nucleated particles.

Higher values of E_g and DG were obtained with BPO than with KPS (Table 2). These differences in the mass of grafted PS could be attributed to two simultaneous effects: (i) the large fraction of homopolystyrene particles produced by secondary nucleation, that contributes to reduce the grafting probability of the KPS initiation system; and (ii) the different ability of the analyzed radicals to induce grafting. Grafting mainly occurs by abstraction of the allylic hydrogens from the PB chains [27–29]; and this reaction is faster with the oxygen-centered radicals produced by decomposition of BPO, than with growing styryl radicals [30]. More specifically, at 90 °C, the chain transfer capacity of BPO primary radicals towards PB was estimated as 1400-fold higher than that of styryl radicals [31]. KPS also gave place to oxygen-centered radicals, but the sulfate radicals produced in the water phase are hydrophilic, and polymerized in the water phase prior to entering as styryl radicals into the organic phases; which in turn induced less grafting than primary BPO radicals and had a reduced probability to react with PB, due to the large fraction of styryl radicals entering to the homopolystyrene particles.

To help interpret the microstructure results, consider the estimated average number of grafting points per copolymer molecule. In the reactions with KPS but without tDM, GP was close to 1, while in the reactions with BPO, the number of grafting points per PB chain was much higher (GP > 7). Thus, KPS induced a reduced grafting of long PS branches, while BPO induced an increased branching of short PS branches that also justified the higher gel content. When increasing the BPO concentration, larger amounts of primary oxygen-centered radicals were generated in the particles. This enhanced grafting, termination reactions, and GP, but decreased the average molecular weights, and maintained E_g and DG almost constant. The addition of CTA in the experiments with KPS did not modify the mass of PS grafted (and therefore E_g and DG), but it significantly increased GP. This could be attributed to a higher grafting ability of the sulfur-centered tDM radicals compared with styryl radicals.

3.3. Particle morphology

Fig. 3 shows the TEM images of latex particles obtained with KPS in experiments $PB_5KPS_{0.75}$, $PB_5KPS_{0.75}C_{0.4}$, and $PB_{10}KPS_{0.75}$. In all cases, most of the particles are homogeneous, and were formed by secondary nucleation. Additionally, the observed hybrid particles exhibit "core–shell" morphologies, and some of them are mostly PB. The larger hybrid particles were formed by droplets nucleation, and have possibly lost most of their monomer by diffusion into the smaller particles formed by secondary nucleation.

Fig. 4 shows the final hybrid particles obtained with BPO in experiments $PB_5BPO_{2.1}$, $PB_8BPO_{2.1}$, and $PB_{10}BPO_{0.75}$. In all cases, similar hybrid morphologies are observed. Most of the particles exhibit an internal rubbery phase, compatible with a particle formation mechanism by droplets nucleation. The larger particles present an internal rubbery phase with multiple PS occlusions, and the smaller particles are more homogeneous and richer in PS, with an internal black ring of PB rich-phase.

The generated graft copolymer in principle stabilized the PS-rich/PB-rich interface, and affected the final morphology. Thus, the high grafting efficiencies and large number of short PS branches in the experiments with BPO, tend to stabilize the PS occlusions in the PB-rich phase, and to produce a multiple-occlusions morphology [28,32]. In contrast, the morphologies of

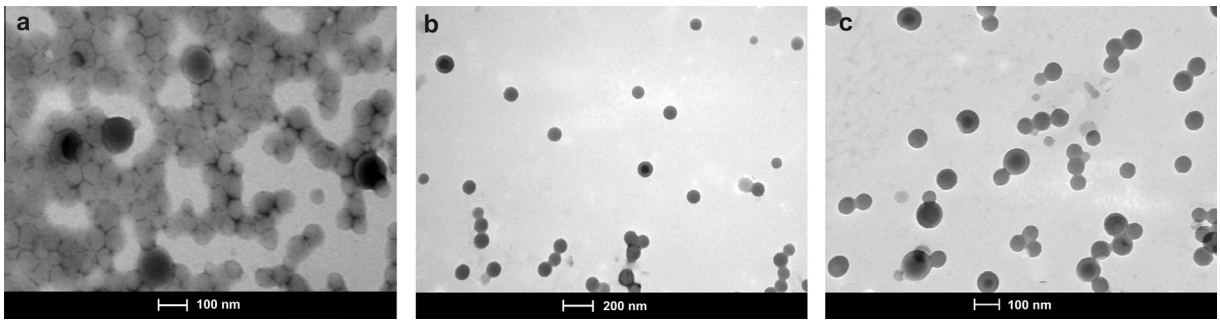

Fig. 3. TEM micrographs of the final latex particles synthesized with KPS: $PB_5KPS_{0.75}$ (a); $PB_5KPS_{0.75}C_{0.4}$ (b); and $PB_{10}KPS_{0.75}$ (c).

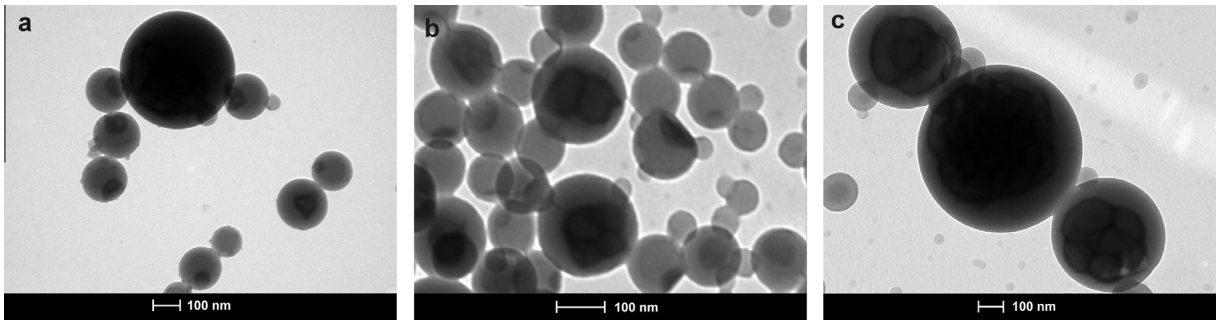

Fig. 4. TEM micrographs of the final hybrid particles of the latexes synthesized with BPO: $PB_5BPO_{2.1}$ (a); $PB_8BPO_{2.1}$ (b); and $PB_{10}BPO_{0.75}$ (c).

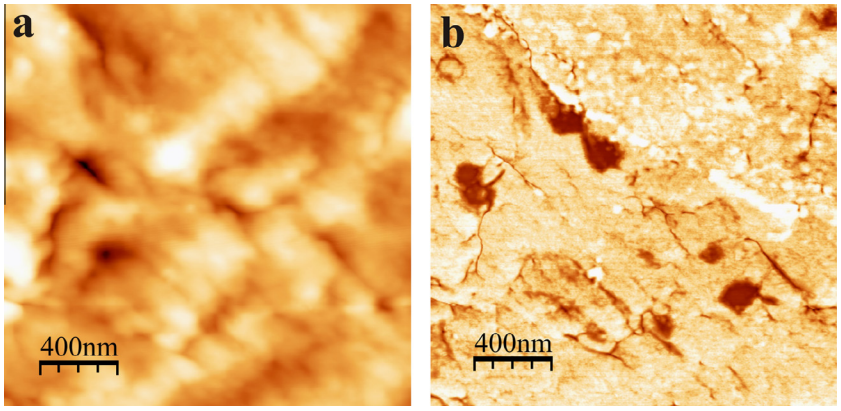

Fig. 5. AFM height (a) and phase (b) images (2 μm × 2 μm) of the cross-section of material obtained by compression at 180 °C for 25 min of the final sample from $PB_{10}KPS_{0.75}$.

the experiments with KPS are the result of the lower grafting efficiencies, longer PS branches, and high secondary nucleation.

3.4. Final material morphology and mechanical properties

Figs. 5 and 6 respectively present the AFM images of the cross-sectional cut materials obtained from $PB_{10}KPS_{0.75}$ and $PB_{10}BPO_{0.75}$. Surface imperfections due to cutting are obvious in both height images (Figs. 5a and 6a), whereas the phase images provide the existence and the contrast of two phases (Figs. 5b and 6b). In the case of the material synthesized with KPS, Fig. 5b shows a continuous hard matrix composed by PS melted with some soft PB particles. This phase distribution is related with the observed morphology of the particles by TEM (Fig. 3c), where PS particles melt together in the continuous phase and the PB core of the hybrid particles became the discrete soft phases. On the other hand, the material produced with BPO do not evidence a continuous PS phase and presents an internal morphology with two different zones: a hard PS phase with irregular form and size and a phase constituted by very small PS particles surrounded by the soft PB (Fig. 6b). Considering the hybrid particles morphology observed by TEM (Fig. 4c), the PB rich phases with multiple PS occlusions agglomerated together giving rise to the heterogeneous zones, while the PS, which is ungrafted and outside of the occlusions, form the irregular PS phases. Furthermore, the sizes of the PS occlusions are similar to those observed inside the hybrid particles by TEM.

Fig. 7 presents the stress–strain curves of the final dry materials; and Table 3 presents the corresponding global values. Also included are the results of a commercial HIPS. The molecular microstructure of the commercial sample was characterized as described before; and yielded the following results: PB content = 7.5 wt%; gel content = 26.5%; E_g = 18.7%; DG = 231%; $\bar{M}_{n,PS}$ = 34,700 g/mol; and $\bar{M}_{w,PS}$ = 146,900 g/mol.

As expected, when increasing the rubber content, a reduction in the elastic modulus and tensile strength is obtained (Table 3 and

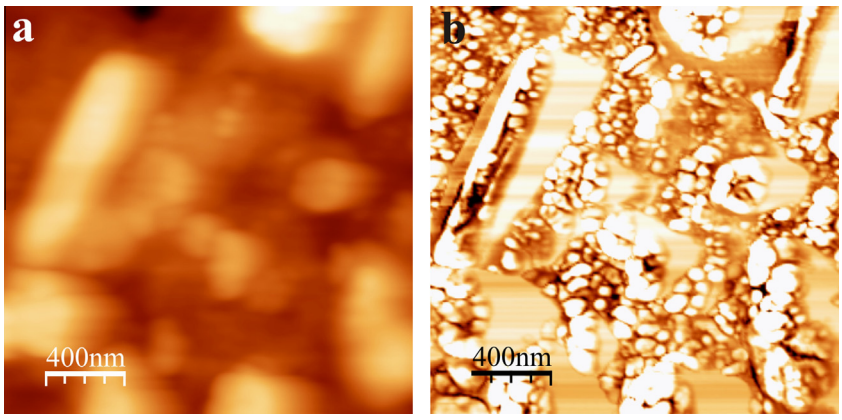

Fig. 6. AFM height (a) and phase (b) images (2 μm × 2 μm) of the cross-section of material obtained by compression at 180 °C for 25 min of the final sample from $PB_{10}BPO_{0.75}$.

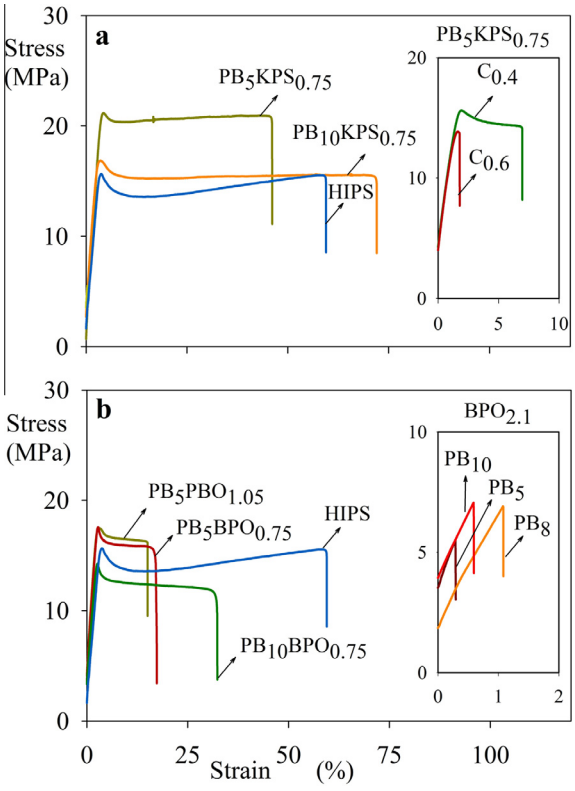

Fig. 7. Tensile stress–strain curves of the final dry toughened PS materials. Products synthesized with KPS (a) and with BPO (b) are compared with a commercial HIPS.

Table 3
Tensile properties of the final dry toughened PS materials and of a commercial HIPS.

Exp.	Young modulus (MPa)	Tensile strength (MPa)	Elongation at break (%)
$PB_5KPS_{0.75}$	765 ± 31	21.0 ± 0.4	47.1 ± 4.8
$PB_5KPS_{0.75}C_{0.4}$	857 ± 27	15.5 ± 0.2	6.9 ± 0.7
$PB_5KPS_{0.75}C_{0.6}$	858 ± 27	13.6 ± 0.7	1.8 ± 0.4
$PB_{10}KPS_{0.75}$	710 ± 26	16.9 ± 0.5	69.1 ± 10.4
$PB_5BPO_{0.75}$	754 ± 19	17.5 ± 0.3	16.1 ± 2.3
$PB_5BPO_{1.05}$	744 ± 19	17.8 ± 0.2	14.6 ± 1.9
$PB_5BPO_{2.1}$	737 ± 27	5.3 ± 0.3	0.34 ± 0.06
$PB_8BPO_{2.1}$	596 ± 15	6.8 ± 1.7	0.88 ± 0.2
$PB_{10}BPO_{0.75}$	582 ± 15	13.9 ± 0.5	32.7 ± 4.8
$PB_{10}BPO_{2.1}$	557 ± 23	6.5 ± 1.3	0.62 ± 0.09
HIPS	598 ± 25	16.0 ± 0.5	57.8 ± 7.8

Fig. 7) [4]. When comparing materials of the same PB content, those synthesized with KPS (and without CTA, $PB_5KPS_{0.75}$ and $PB_{10}KPS_{0.75}$) exhibit higher elastic modulus and tensile strengths with respect to the materials synthesized with BPO, probably due to their longer PS chains [4]. While molecular weights of the free PS affect elastic modulus and tensile strengths, elongantion and toughness are mainly determined by the material morphology and its molecular microstructure. Higher elongation and toughness obtained with KPS are due to the soft phase is arranged as discrete particles, reinforcing the hard PS matrix, while this desired distribution is not present in the BPO material.

The incorporation of tDM in experiments $PB_5KPS_{0.75}C_{0.4}$ and $PB_5KPS_{0.75}C_{0.6}$ with KPS, considerably lowered tensile strength and elongation at break. The addition of CTA did not modify the hybrid particles morphology, but significantly reduced the average molecular weights of the free PS. Also, the low diffusion rate of tDM from the droplet-nucleated particles into the secondary nucleated particles would produce shorter PS branches compared to the longer free PS chains. In such case, the low molecular weights of the grafted branches could not efficiently compatibilize (i.e., entangle) the dispersed rubbery phase to the main free PS phase, reducing the material toughness [8]. When employing CTA, the highest elongation at break was obtained with 0.4% of CTA, due to the longer PS chains (both free and grafted).

The polymer obtained with high BPO concentration (of 2.1% wbm) was relatively brittle, with low tensile strength and elongation at break. However, both properties were improved when reducing the BPO content between 0.75 and 1.05% wbm, which in turn increased the molecular weights of the (free and grafted) PS chains. All of these materials exhibited similar particle morphologies, suggesting that the poorer mechanical performances of the materials obtained with a high BPO content are due to the reduced molecular weights of both the free PS and the PS branches. Finally, note that the toughest materials were obtained with KPS but without tDM, where the morphology presented the soft phases discretely distributed into a PS matrix and the PS chains (free and branches) were long enough to improve entanglement, showing mechanical properties similar to those of a commercial HIPS.

4. Conclusions

PB-toughened PS nanoparticles were synthesized through high-solids miniemulsion polymerization. The water-soluble KPS initiator induced a significant secondary nucleation, while the oil-soluble BPO initiator favored droplets nucleation. Compared to reactions with KPS, the BPO systems tended to pseudo-bulk

polymerization, with enhanced termination and reduced PS molecular weights.

The amount of grafted PS and the particle morphologies were also affected by the initiator type. While KPS generated low grafting and hybrid particles off "core–shell" morphology, BPO induced a relatively higher degree of grafting, and hybrid particles with stabilized vitreous occlusions in the rubber phase.

The material morphology and the molecular weights of free PS and grafted branches determined the tensile properties of the synthesized materials. The miniemulsion polymerization obtained with KPS, where only a small percentage of the particles are hybrid and come from the droplets, give rise to a material with a PS matrix, constituted by the secondary nucleated particles, with medium size rubber particles that acts as reinforcing component. However, the low molecular weight of grafted PS obtained in the experiments with KPS and CTA, reduced the materials toughness due to an inefficient entanglement between phases. On the other hand, the use of BPO achieved the nearest situation to the ideal one to one copy nucleation, where most of the particles have a morphology of multi PS occlusions, which is then reproduced in the melt material, without evidencing a continuous PS phase, and reducing the reinforcing effects. Also, the lower molecular weights observed with high BPO content produced brittle materials of reduced elastic modulus, tensile strength, and elongation at break; but these properties were considerably improved when reducing the BPO concentration.

The described miniemulsion process enabled the synthesis of nanostructured and toughened polystyrenes, of mechanical properties similar to those of a commercial HIPS, but with the advantages of aqueous emulsion/miniemulsion polymerizations that avoid the use of organic solvents and admit high monomer conversions, while improving the typical mixing and heat transfer problems of bulk (or quasi-bulk) processes even working at high solid contents. Another advantage of the described high-conversion process is the potential application of a post-polymerization stage, to almost completely eliminate residual monomer.

Acknowledgements

We acknowledge the following Argentine institutions for their financial support: CONICET, ANPCyT, Universidad Nacional del Litoral, and Secretaría de Políticas Universitarias del Ministerio de Educación. In addition, we acknowledge Dr. Julia Yañez (TEM service, CCT-CONICET-Bahía Blanca, Argentina) for her help with the TEM observations; and M.C. Brandolini and J.L. Castañeda (INTEC) for their help with the SEC measurements.

References

[1] I. Yamaoka, Toughened polymer blends composed of a ductile styrene-butadiene-styrene matrix with brittle methyl methacrylate-styrene particles, Polymer 36 (1995) 3359–3368.
[2] H. Keskkula, D.R. Paul, K.M. McCreedy, D.E. Henton, Methyl methacrylate grafted rubbers as impact modifiers for styrenic polymers, Polymer 28 (1987) 2063–2069.
[3] M.F. Martin, J.P. Viola, J.R. Wuensch, Preparation, properties and applications of high-impact polystyrene, in: J. Scheirs, D. Priddy (Eds.), Modern Styrenic Polymers: Polystyrenes and Styrenic Copolymers, Wiley Series in Polymer Science, John Wiley & Sons Ltd, England, 2003, pp. 247–280.
[4] G.R. Meira, D.A. Estenoz, C.V. Luciani, Continuous bulk process for the production of high-impact polystyrene: recent developments in modeling and control, Macromol. React. Eng. 1 (2007) 25–39.
[5] M. Jiang, X. Huang, T. Yu, Phase separation in blends of homopolymer and graft copolymer based on styrene and butadiene, Polymer 24 (1983) 1259–1266.
[6] T. Inoue, T. Soen, T. Hashimoto, H. Kawai, Studies on domain formation of the A-B-type block copolymer from its solutions. Ternary polymer blend of the styrene-isoprene block copolymer with polystyrene and polyisoprene, Macromolecules 3 (1970) 87–92.
[7] M. Jiang, H. Xie, Miscibility and morphology in block copolymer/homopolymer blends, Prog. Polym. Sci. 16 (1991) 977–1026.
[8] T. Cavanaugh, K. Buttle, J. Turner, B. Nauman, The study of various styrene-butadiene copolymers as compatibilisers in bulk blends of polystyrene/polybutadiene, Polymer 39 (1998) 4191–4197.
[9] G. Gao, C. Zhou, H. Yang, H. Zhang, Influence of core-shell rubber particles synthesized with different initiation systems on the impact toughness of modified polystyrene, J. Appl. Polym. Sci. 103 (2007) 738–744.
[10] G. Gao, J. Zhang, H. Yang, C. Zhou, H. Zhang, Deformation mechanism of polystyrene toughened with sub micrometer monodisperse rubber particles, Polym. Int. 55 (2006) 1215–1221.
[11] G.D. Cai, H.Y. Yang, L.D. Zhu, H. Liu, G.F. Wu, M.Y. Zhang, C. Zhou, G.H. Gao, H.X. Zhang, Toughening polystyrene by core–shell grafting copolymer polybutadiene-graft-polystyrene with potassium persulfate as initiator, J. Ind. Eng. Chem. 19 (2013) 823–828.
[12] P. Jeong, V.L. Dimonie, E.S. Daniels, M.S. El-Aasser, Hybrid composites latexes, ACS Symp. Ser. 801 (2002) 357–373.
[13] L.I. Ronco, R.J. Minari, J.R. Vega, G.R. Meira, L.M. Gugliotta, Incorporation of polybutadiene into waterborne polystyrene nanoparticles via miniemulsion polymerization, Eur. Polym. J. 49 (2013) 2634–2644.
[14] M.J. Unzué, J.M. Asua, Semicontinuous miniemulsion terpolymerization: effect of the operation conditions, J. Appl. Polym. Sci. 49 (1993) 81–90.
[15] J.R. Leiza, E.D. Sudol, M.S. El-Asser, Preparation of high solids content poly(n-butyl acrylate) latexes through miniemulsion polymerization, J. Appl. Polym. Sci. 64 (1997) 1797–1809.
[16] M. Goikoetxea, I. Beristain, R.J. Minari, M. Paulis, M.J. Barandiaran, J.M. Asua, Continuous miniemulsification for the industrialization of miniemulsion polymerization, Chem. Eng. J. 170 (2011) 114–119.
[17] M. Kurata, Y. Tsunashima, Viscosity – molecular weight relationship and unperturbed dimensions of linear chain molecules, in: J. Brandrup, E.H. Immergut, E.A. Grulke (Eds.), Polymer Handbook, John Wiley & Sons, New York, 1999, pp. VII 1–VII 83.
[18] L.I. Ronco, R.J. Minari, L.M. Gugliotta, Particle nucleation using different initiators in the miniemulsion polymerization of styrene, Braz. J. Chem. Eng. 32 (1) (2015) (in press).
[19] C. Autran, J.C. de la Cal, J.M. Asua, Miniemulsion polymerization kinetics using oil-soluble initiator, Macromolecules 40 (2007) 6233–6238.
[20] F.M. Peng, Polybutadiene grafting and crosslinking in high-impact polystyrene bulk thermal process, J. Appl. Polym. Sci. 40 (1990) 1289–1302.
[21] L.C. Sawyer, D.T. Grubb, G.F. Meyers (Eds.), Polymer Microscopy, third ed., Springer, 2008.
[22] I. Horcas, R. Fernandez, J.M. Gomez-Rodriguez, J. Colchero, J. Gomez-Herrero, A.M. Baro, WSXM: a software for scanning probe microscopy and a tool for nanotechnology, Rev. Sci. Instrum. 78 (2007) 013705.
[23] J.M. Asua, Miniemulsion polymerization, Prog. Polym. Sci. 27 (2002) 1283–1346.
[24] R.J. Minari, J.R. Vega, M. Gonzáles-Sierra, G.R. Meira, L.M. Gugliotta, Emulsion polymerization of styrene with iso-octyl-3-mercaptopropionate as chain transfer agent, J. Appl. Polym. Sci. 109 (2008) 3944–3952.
[25] C. Costa, S.A.S. Timmermann, J.C. Pinto, P.H.H. Araujo, C. Sayer, Compartmentalization effects on miniemulsion polymerization with oil-soluble initiator, Macromol. React. Eng. 7 (2013) 221–231.
[26] A. Salazar, L.M. Gugliotta, J.R. Vega, G.R. Meira, Molecular weight control in a starved emulsion polymerization of styrene, Ind. Eng. Chem. Res. 37 (1998) 3582–3591.
[27] N.-J. Huang, D.C. Sundberg, Fundamental Studies of Grafting Reactions in Free Radical Copolymerization. III. Grafting of styrene, acrylate, and methacrylate monomers onto cis-polybutadiene using benzoyl peroxide initiator in solution polymerization, J. Polym. Sci. A Polym. Chem. 33 (1995) 2571–2586.
[28] G.P. Leal, J.M. Asua, Evolution of the morphology of HIPS particles, Polymer 50 (2009) 68–76.
[29] R.J. Minari, M. Goikoetxea, I. Beristain, M. Paulis, M.J. Barandiaran, J.M. Asua, Post-polymerization of waterborne alkyd/acrylics. Effect on polymer architecture and particle morphology, Polymer 50 (2009) 5892–5900.
[30] G. Moad, D.H. Solomon, The Chemistry of Free Radical Polymerization, Elsevier Science, 1995.
[31] D.A. Estenoz, E. Valdez, H.M. Oliva, G.R. Meira, Bulk polymerization of styrene in presence of polybutadiene: calculation of molecular macrostructure, J. Appl. Polym. Sci. 59 (1996) 861–885.
[32] M. Vonka, J. Kosek, Modelling the morphology evolution of polymer materials undergoing phase separation, Chem. Eng. J. 207–208 (2012) 895–905.